Article

Covalent Attachment of a Transition Metal Coordination Complex to Functionalized Oligo(phenylene-ethynylene) Self-Assembled Monolayers

Abhishek Dube, Andrew R. Chadeayne, Manish Sharma, Peter T. Wolczanski, and James R. Engstrom

J. Am. Chem. Soc., **2005**, 127 (41), 14299-14309• DOI: 10.1021/ja054378e • Publication Date (Web): 23 September 2005

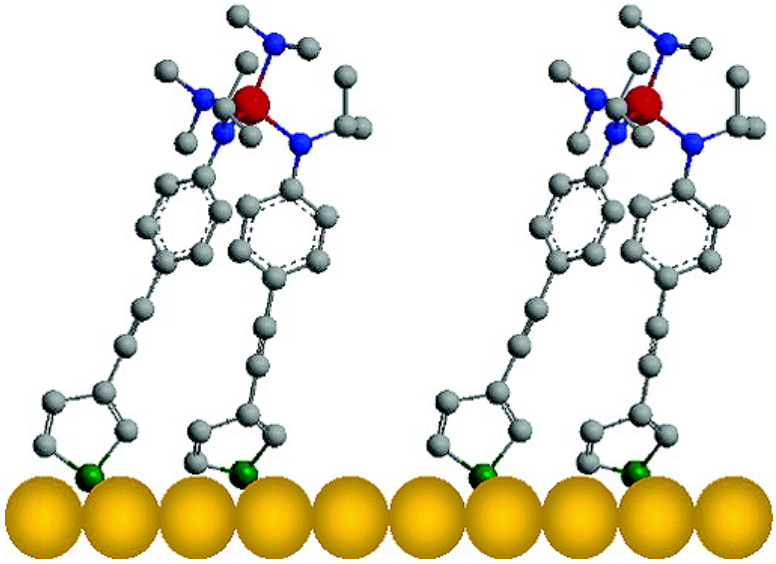

More About This Article

Additional resources and features associated with this article are available within the HTML version:

- Supporting Information
- Links to the 8 articles that cite this article, as of the time of this article download
- Access to high resolution figures
- Links to articles and content related to this article
- Copyright permission to reproduce figures and/or text from this article

View the Full Text HTML

J|A|C|S
ARTICLES
Published on Web 09/23/2005

Covalent Attachment of a Transition Metal Coordination Complex to Functionalized Oligo(phenylene-ethynylene) Self-Assembled Monolayers

Abhishek Dube,[†] Andrew R. Chadeayne,[‡] Manish Sharma,[†]
Peter T. Wolczanski,[‡] and James R. Engstrom*,[†]

Contributions from the School of Chemical and Biomolecular Engineering, and Department of Chemistry and Chemical Biology, Cornell University, Ithaca, New York 14853

Received July 1, 2005; E-mail: jre7@cornell.edu

Abstract: We have investigated the reaction of tetrakis(dimethylamido)titanium, $Ti[N(CH_3)_2]_4$, with *N*-isopropyl-*N*-[4-(thien-3-ylethynyl) phenyl] amine and *N*-isopropyl-*N*-(4-{[4-(thien-3-ylethynyl) phenyl]ethynyl}-phenyl) amine self-assembled monolayers (SAMs), on polycrystalline Au substrates. The structure of the SAMs themselves has also been investigated. Both molecules form SAMs on polycrystalline Au bound by the thiophene group. The longer-molecular-backbone molecule forms a denser SAM, with molecules characterized by a smaller tilt angle. X-ray photoelectron spectroscopy (XPS) and angle-resolved XPS have been employed to examine the kinetics of adsorption, the spatial extent of reaction, and the stoichiometry of reaction. For both the SAMs, adsorption is described well by first-order Langmuirian kinetics, and adsorption is self-limiting from $T_s = -50$ to 30 °C. The use of angle-resolved XPS clearly demonstrates that the $Ti[N(CH_3)_2]_4$ reacts exclusively with the isopropylamine end group via ligand exchange, and there is no penetration of the SAM, followed by reaction at the SAM−Au interface. Moreover, the SAM molecules remain bound to the Au surface via their thiopene functionalites. From XPS, we have found that, in both cases, approximately one $Ti[N(CH_3)_2]_4$ is adsorbed per two SAM molecules.

Introduction

Most modern electronic devices are solid-state devices, the active components of which are constructed essentially entirely of inorganic materials—semiconductors, metals, various oxides, nitrides, and silicides. To date, excepting important applications such as photoresists in lithography, organic materials have played a rather secondary role in this technology. This situation is changing, and considerable interest has developed in the past 5−10 years concerning the use of small molecules in active components of electronic circuitry—the field is known as molecular-scale electronics or molecular electronics.[1] A major challenge in this area is devising chemistries and processes that can bring together these two diverse materials sets, inorganic and organic, without doing damage to the delicate organic structures and functionalities.

Attempts to construct devices incorporating molecules have taken many designs: break junctions, formed mechanically[2] and electrically,[3] nanopores,[4] and cross-bar arrays[5] are perhaps the most well-known examples. In all these cases, the so-called bottom contact is formed using chemically specific adsorption, alternatively referred to as self-assembly. The solution-phase deposition of organothiols on gold[6] is a well-developed chemistry for forming well-ordered self-assembled monolayers (SAMs). These SAMs can have rigid backbones comprised of aromatic fragments[7] or "floppy" backbones comprised of aliphatic fragments.[8] The former, including oligo(phenylene-ethynylene) SAMs, have attracted interest due to their structure, which should promote facile electrical conduction along their molecular backbone. Indeed, conjugated SAMs have been used for making sensors,[9] rectifiers,[10,11] and molecular switches.[12] A common motif in these devices is an electrode/molecule/electrode microstructure, formed by sequential deposition and patterning steps.[4,5,11,12]

It is important to note, however, that with all these approaches a second or top contact with the SAM (an inorganic-on-organic interface) is required to fabricate functional molecular electronic

[†] School of Chemical and Biomolecular Engineering, Cornell University.
[‡] Department of Chemistry and Chemical Biology, Cornell University.

(1) Reed, M. A.; Tour, J. M. *Sci. Am.* **2000**, 86−93.
(2) Reed, M. A.; Zhou, C.; Muller, C. J.; Burgin, T. P.; Tour, J. M. *Science* **1997**, *278*, 252−254.
(3) Park, J.; Pasupathy, A. N.; Goldsmith, J. I.; Chang, C.; Yaish, Y.; Petta, J. R.; Rinkoski, M.; Sethna, J. P.; Abruña, H. D.; McEuen, P. L.; Ralph D. C. *Nature* **2002**, *417*, 722−725.
(4) Ralls, K. S.; Buhrman, R. A.; Tiberio, R. C. *Appl. Phys. Lett.* **1989**, *55*, 2459−2561.
(5) Chen, Y.; Ohlberg, D. A. A.; Li, X.; Stewart, D. R.; Williams, R. S.; Jeppesen, J. O.; Nielsen, K. A.; Stoddart, J. F.; Olynick, D. L.; Anderson, E. *Appl. Phys. Lett.* **2003**, *82*, 1610−1612.
(6) Nuzzo, R. G.; Allara, D. L. *J. Am. Chem. Soc.* **1983**, *105*, 4481−4483.
(7) Bain, C. D.; Troughton, E. B.; Tao, Y.-T.; Evall, J.; Whitesides, G. M.; Nuzzo, R. G. *J. Am. Chem. Soc.* **1989**, *111*, 321−335.
(8) Tour, J. M.; Jones, L., II; Pearson, D. L.; Lamba, J. J. S.; Burgin, T. P.; Whitesides, G. M.; Allara, D. L.; Parikh, A. N.; Atre, S. V. *J. Am. Chem. Soc.* 1995, *117*, 9529−9534.
(9) Hutchinson, J. E.; Postlethwaite, T. A.; Murray, R. W. *Langmuir* **1993**, *9*, 3277−3283.
(10) Martin, A. S.; Sambles, J. R.; Ashwell, G. J. *Phys. Rev. Lett.* **1993**, *70*, 218−221.
(11) Metzger, R. M.; Xu, T.; Peterson, I. R. *J. Phys. Chem. B* **2001**, *105*, 7280−7290.
(12) Chen, J.; Reed, M. A.; Rawlett, A. M.; Tour, J. M. *Science* **1999**, *286*, 1550−1552.

devices. The tip of either a conducting atomic force microscope (c-AFM) or a scanning tunneling microscope (STM) has been used to make this contact.[13−15] This approach can work well for fundamental studies of single to several hundred molecules, but it obviously does not make a permanent contact and is, in general, unsuitable for fabricating arrays of devices. Formation of inorganic or metal thin films on SAMs, whether explicitly for top contacts or not, has mostly involved evaporative deposition in a vacuum or liquid-phase deposition. Vapor deposition of elemental metals (e.g., Ag, Cu, Ti, Al, Fe, Cr, and Au) on SAMs possessing different terminal organic functional groups (OFGs) such as $-CH_3$, $-OH$, $-COOH$, $-COOCH_3$, $-CN$, and $-SH$ has been studied extensively.[16−24] In many cases, due to the rather unspecific reactions of many of these elemental metals, mixed adlayers were formed because reactions occurred not only with the OFG tail groups but also apparently with the SAM backbone and headgroups. Such penetration of the organic monolayer by the metal species, the extent of which depended on the terminal OFG, as well as the metal studied, is unacceptable concerning most devices envisaged for molecular electronics. Formation of inorganic-on-organic interfaces via liquid-phase thin-film deposition has also been problematic. TiO_2 thin films have been deposited on alkyltrichlorosilane SAMs possessing different terminal OFGs.[25−28] The films, in most instances, were rough and exhibited poor adhesion, while molecular-level details concerning the interfaces were absent from these studies. Finally, X-ray photoelectron spectroscopy (XPS) revealed that the films suffered from carbon and chlorine contamination.[28]

Formation of inorganic−organic interfaces via the use of transition metal coordination complexes holds tremendous promise. A key is to tailor both the terminal OFG and the transition metal complex such that they react with each other in a specific fashion. Growth that is self-limiting may also be desirable and feasible with this approach, as uncontrolled continuous deposition might lead to degradation of the interface. There are a handful of studies that have examined the deposition of metal thin films on SAMs (thiols), including Au growth via $[(CH_3)_3P]AuCH_3$,[29] Pd growth via Cp(allyl)Pd,[29c,30] and Al growth via $[(CH_3)_3N]AlH_3$.[31,32] In the case of Au and Pd deposition, the selectivity of growth and film morphology were examined. In the case of Al deposition,[31] interfacial chemistry was examined using XPS, but an explicit examination of the kinetics of adsorption was not attempted. Recently, we have completed what is perhaps the most rigorous study of the reaction of a transition metal coordination complex with SAMs,[33] in this case, the reaction of tetrakis(dimethylamido)-titanium, $Ti[N(CH_3)_2]_4$, a TiN precursor,[34−41] with alkyltrichlorosilane SAMs possessing $-OH$, $-NH_2$, and $-CH_3$ terminal OFGs. We found by XPS that the reaction was self-limiting in all these cases. Using angle-resolved XPS (ARXPS) to probe the spatial extent of the reaction, we found that penetration of the SAM followed by reaction at the SAM/substrate occurred in the case of the $-CH_3$ SAM. In the case of the $-NH_2$ SAM, however, no evidence of penetration was found, and reaction was confined to the terminal $-NH_2$ group.

In this work, we consider the reaction of $Ti[N(CH_3)_2]_4$ with adsorbed molecules that possess specially chosen head and tail groups and backbone. In particular, a thiophene headgroup has been chosen for its affinity for Au surfaces, an isopropylamine terminal OFG to react with $Ti[N(CH_3)_2]_4$, and a phenylene-ethynylene backbone for electrical conduction. Although a specific device function is not assumed here, this scheme leads to the aforementioned electrode/molecule/electrode structural motif used in molecular switches[5,12] and rectifiers.[11] Thiophenes offer potential advantages over the related thiols. For example, thiols may be reduced to thiolates[42] or oxidized to disulfides,[43] whereas the likelihood of a thiophene group participating in reactions other than simple molecular adsorption, under our reaction conditions, is quite small due to its stable ring structure. Comparative studies of thiophene SAMs and thiol SAMs on Au are relatively scarce. STM has been used to demonstrate that thiophene can form well-ordered monolayers on Au(111).[44] In another study, the structural evolution of a thiophene SAM

(13) Cui, X. D.; Primak, A.; Zarate, X.; Tomfohr, J.; Sankey, O. F.; Moore, A. L.; Moore, T. A.; Gust, D.; Harris, G.; Lindsay, S. M. *Science* **2001**, *294*, 571−574.
(14) Ng, M. K.; Lee, D. C.; Yu, L. *J. Am. Chem. Soc.* **2002**, *124*, 11862−11863.
(15) Bumm, L. A.; Arnold, J. J.; Cygan, M. T.; Dunbar, T. D.; Burgin, T. P.; Jones, L., II; Allara, D. L.; Tour, J. M.; Weiss, P. S. *Science* **1996**, *271*, 1705−1707.
(16) Jung, D. R.; Czanderna, A. W. *Crit. Rev. Solid State Mater. Sci.* **1994**, *19*, 1−54.
(17) Herdt, G. C.; Jung, D. R.; Czanderna, A. W. *Prog. Surf. Sci.* **1995**, *50*, 103−129.
(18) Tarlov, M. J. *Langmuir* **1992**, *8*, 80−89.
(19) Ohgi, T.; Sheng, H.-Y.; Dong, Z.-C.; Nejoh, H. *Surf. Sci.* **1999**,*442*, 277−282.
(20) Fisher, G. L.; Hooper, A. E.; Opila, R. L.; Allara, D. L.; Winograd, N. *J. Phys. Chem. B* **2000**, *104*, 3267−3273.
(21) Konstadinidis, K.; Zhang, P.; Opila, R. L.; Allara, D. L. *Surf. Sci.* **1995**, *338*, 300−312.
(22) Hooper, A. E.; Fisher, G. L.; Konstadinidis, K.; Jung, D.; Nguyen, H.; Opila, R. L.; Collins, R. W.; Winograd. N.; Allara, D. L. *J. Am. Chem. Soc.* **1999**, *121*, 8052−8064.
(23) Fisher, G. L.; Walker, A. V.; Hooper, A. E.; Tighe, T. B.; Bahnck, K. B.; Skriba, H. T.; Reinard, M. D.; Haynie, B. C.; Opila, R. L.; Winograd, N.; Allara, D. L. *J. Am. Chem. Soc.* **2002**, *124*, 5528−5541.
(24) Carlo, S. R.; Wagner, A. J.; Fairbrother, D. H. *J. Phys. Chem. B* **2000**, *104*, 6633−6641.
(25) Shin, H.; Collins, R. J.; De Guire, M. R.; Heuer, A. H.; Sukenik, C. N. *J. Mater. Res.* **1995**, *10*, 692−698.
(26) Shin, H.; Collins, R. J.; De Guire, M. R.; Heuer, A. H.; Sukenik, C. N. *J. Mater. Res.* **1995**, *10*, 699−703.
(27) Niesen, T. P.; Bill, J.; Aldinger, F. *Chem. Mater.* **2001**, *13*, 1552−1559.
(28) Masuda, Y.; Jinbo, Y.; Yonezawa, T.; Koumoto, K. *Chem. Mater.* **2002**, *14*, 1236−1241.
(29) (a) Wohlfart, P.; Weiss, J.; Kashammer, J.; Winter, C.; Scheumann, V.; Fischer, R. A.; Mittler-Nehera, S. *Thin Solid Films* **1999**, *340*, 274−279. (b) Winter, C.; Weckenmann, U.; Fischer, R. A.; Kashammer, J.; Scheumann, V.; Mittler, S. *Chem. Vap. Depn.* **2000**, *6*, 199−205. (c) Fischer, R. A.; Weckenmann, U.; Winter, C.; Käshammer, J.; Scheumann, V.; Mittler, S. *J. Phys. IV: Proc.* **2001**, *11*, Pr3/1183−Pr3/1190.
(30) Weckenmann, U.; Mittler, S.; Krämer, S.; Aliganga, A. K. A.; Fischer, R. A. *Chem Mater.* **2004**, *16*, 621−628.
(31) Weiss, J.; Himmel, H. J.; Fischer, R. A.; Woell, C. *Chem. Vap. Deposition* **1998**, *4*, 17−21.
(32) Wohlfart, P.; Weiss, J.; Käshmmer, J.; Kreiter, M.; Winter, C.; Fischer, R.; Mittler-Neher, S. *Chem. Vap. Deposition* **1999**, *5*, 165−170.
(33) Killampalli, A. S.; Ma, P. F.; Engstrom, J. R. *J. Am. Chem. Soc.* **2005**, *127*, 6300−6310.
(34) Fix, R.; Gordon, R. G.; Hoffman, D. M. *Chem. Mater.* **1991**, *3*, 1138−1148.
(35) Musher, J. N.; Gordon, R. G. *J. Mater. Res.* **1996**, *11*, 989−1001.
(36) Ritala, M.; Asikainen, T.; Leskelä, M.; Jokinen, J.; Lappalainen, R.; Utriainen, M.; Niinistö, L.; Ristolainen, E. *Appl. Surf. Sci.* **1997**, *120*, 199−212.
(37) Berry, A.; Mowery, R.; Turner, N. H.; Seitzman, L.; Dunn, D.; Ladouceur, H. *Thin Solid Films* **1998**, *323*, 10−17.
(38) Min, J.-S.; Park, J.-S.; Park, H.-S.; Kang, S.-W. *J. Electrochem. Soc.* **2000**, *147*, 3868−3872.
(39) Ritala, M.; Asikainen, T.; Leskelä, M.; Dekker, J.-P.; Mutsaers, C.; Soininen, P. J.; Skarp, J. *Chem. Vap. Deposition* **1999**, *5*, 7−9.
(40) Elam, J. W.; Wilson, C. A.; Schuisky, M.; Sechrist, Z. A.; George, S. M. *J. Vac. Sci. Technol. B* **2003**, *21*, 1099−1107.
(41) Elam, J. W.; Schuisky, M.; Ferguson, J. D.; George, S. M. *Thin Solid Films* **2003**, *436*, 145−156.
(42) Biebuyck, H. A.; Bain, C. D.; Whitesides, G. M. *Langmuir* **1994**, *10*, 1825−1831.
(43) Fenter, P.; Eberhardt, A.; Eisenberger, P. *Science* **1994**, *266*, 1216−1218.
(44) Dishner, M. H.; Hemminger, J. C.; Feher, F. J. *Langmuir* **1996**, *12*, 6176−6178.

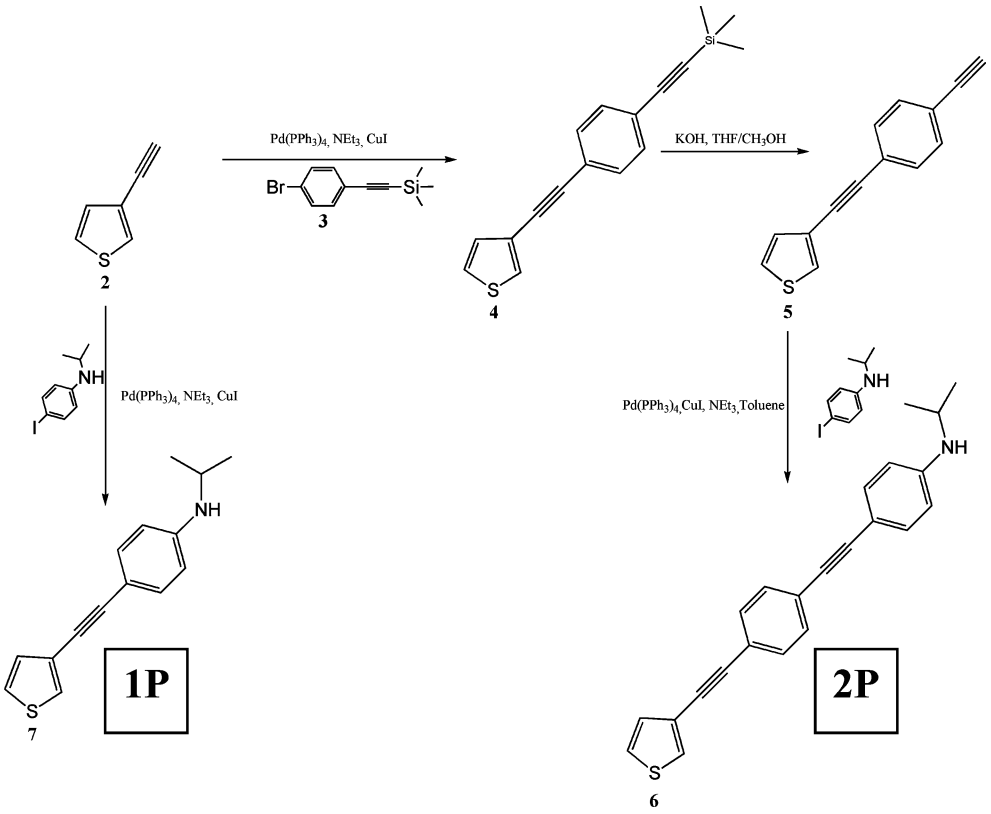

Figure 1. Schematic for the synthesis of *N*-isopropyl-*N*-[4-(thien-3-ylethynyl) phenyl] amine and *N*-isopropyl-*N*-(4-{[4-(thien-3-ylethynyl) phenyl] ethynyl} phenyl) amine.

on Au(111) was examined by Fourier transform infrared reflection absorption spectroscopy.[45] The formation of the SAM was found to occur in two stages: in the first stage, thiophene orients parallel to the Au surface; in the second stage, the molecular orientation changes to upright. In other work, XPS[46] revealed that the sulfur in thiophene chemically interacts with Au, indicated by a shift in the binding energy of the $S(2p_{3/2})$ by 2−3 eV.

Herein, we describe our studies of the following: the synthesis and formation of SAMs possessing a molecular backbone that should facilitate facile electrical conduction and an endgroup that should bind in a specific fashion to a Au substrate; the reactions between the organic functional tailgroups of these SAMs [-NH(i-C_3H_7)] and a transition metal coordination complex, $Ti[N(CH_3)_2]_4$. We use XPS to probe the nature of SAMs that are formed, quantify the kinetics of adsorption of the Ti complex on these layers, and determine the specificity and/or spatial extent of reaction between the Ti complex and the SAMs. Ultimately, this strategy could be used to make "sandwich" structures comprising electrode/molecule/electrode, or any of a variety of structures where precisely fabricated inorganic−organic interfaces are key structural elements.

II. Experimental Section

Complete details concerning the experimental procedures employed here are in the Supporting Information, and we only give a brief summary here. The thiophene ligands, *N*-isopropyl-*N*-[4-(thien-3-ylethynyl) phenyl] amine and *N*-isopropyl-*N*-(4-{[4-(thien-3-ylethynyl) phenyl]ethynyl}phenyl) amine were synthesized using the scheme that is shown in Figure 1. Details of the synthetic procedure, as well as all assignments of the chemical shifts from NMR, are in the Supporting Information. One ligand (**7**) has one phenyl ring in its backbone, whereas the other has two (**6**). From now on, we will use the shorthand notation **1P** for the former and **2P** for the latter, in an obvious reference to the number of phenyl groups in the molecule. SAMs of these thiophene ligands and 4-aminothiophenol were prepared on evaporated gold substrates via a liquid-phase deposition process. Contact angle measurements, ellipsometry, and X-ray photoelectron spectroscopy (XPS) were employed to characterize the order, thickness, and composition of these monolayers. Characterization of the SAMs via XPS and their reactions with $Ti[N(CH_3)_2]_4$ were carried out in a custom built ultrahigh vacuum (UHV) chamber that is described in detail elsewhere.[47]

III. Results and Discussion

A. Characterization of the SAMs. We have used contact-angle measurements, ellipsometry, and XPS to characterize the layers formed from the adsorption of the two molecules of interest on polycrystalline Au. In Table 1, we present data for the advancing and receding contact angles of water, as well as the hysteresis for both of the SAMs. As may be seen, we observe a smaller contact angle for the **1P** SAM in comparison to the **2P** SAM. These results are in qualitative agreement with results reported for thiol SAMs possessing conjugated backbones of varying lengths.[48] In particular, in this work, it was reported that increasing the chain length of the conjugated thiols reduced the tilt angle, which in turn, resulted in a more hydrophobic

(45) Matsuura, T.; Nakajima, M.; Shimoyama, Y. *Jpn. J. Appl. Phys.* **2001**, *40*, 6945−6950.
(46) Noh, J.; Ito, E.; Nakajima, K.; Kim, J.; Lee, H.; Hara, M. *J. Phys. Chem. B* **2002**, *106*, 7139−7141.
(47) Xia, L.-Q.; Jones, M. E.; Maity, N.; Engstrom, J. R. *J. Vac. Sci. Technol. A* **1995**, *13*, 2651−2664.
(48) De Boer, B.; Meng, H.; Perepichka, D. F.; Zheng, J.; Frank, M. M.; Chabal, Y.; Bao, Z. *Langmuir* **2003**, *19*, 4272−4284.

Table 1. Properties of Self-Assembled Monolayers

SAM	contact angle			thickness (ellipsometry)	molecular length	density (cm^{-2}, XPS)
	advancing	receding	hysteresis			
1P	56° ± 3°	41° ± 2°	15°	6.6 ± 0.4 Å	12.6 Å	$2.11 \pm 0.87 \times 10^{14}$
2P	66° ± 1°	56° ± 2°	10°	16.6 ± 0.8 Å	19.6 Å	$3.42 \pm 0.79 \times 10^{14}$
4-aminothiophenol	27° ± 3°			10.7 ± 0.8 Å	5.6 Å	$3.24 \pm 0.91 \times 10^{14}$

character of the longer ring system. Indeed, the ellipsometric data, also shown in Table 1, confirms this picture. The measured ellipsometric thicknesses for the **1P** and **2P** SAMs are 6.6 ± 0.4 and 16.6 ± 0.8 Å, respectively, vs estimated lengths (from molecular models) of 12.6 and 19.6 Å for the molecules themselves. These results are in good qualitative agreement with data for other conjugated thiol SAMs,[48] and the larger tilt angle implicated for the shorter **1P** SAM can be attributed to weaker intermolecular forces due to fewer aromatic rings in the backbone.[49]

Survey XP spectra have been collected from both SAMs, and the following peaks have been observed: Au(4f), N(1s), C(1s), and S(2p). The survey scan was followed by detailed scans for all of these. The C(1s) feature can be used to estimate the absolute coverage of the SAMs. To accomplish this, one needs to account for the photoelectron cross-sections, σ, for the C(1s) and the Au($4f_{7/2}$) peaks, the analyzer transmission, $T(E)$, which is inversely proportional to the kinetic energy (E = 968.6 and 1169.6 eV, respectively), the atomic density of the two elements, N, and the inelastic mean free path, λ, for the photoelectrons. Concerning these, $\sigma_{Au}/\sigma_C = 9.8$,[50] $N_{Au} = 5.88 \times 10^{22}$ atoms·cm^{-3},[51] and $\lambda_{Au} = 15.5$ Å.[52] The atomic density of C in the SAM depends on the coverage or density of the SAM, n_{SAM} (molecules·cm^{-2}), and the mean spacing between C in the backbone, d_C. The integrated intensity of the Au ($4f_{7/2}$) peak for a clean Au substrate is proportional to $\sigma_{Au}N_{Au}\lambda_{Au}T(E_{Au})$. For the C(1s) peak, we must account for the finite thickness of the layer, and the integrated intensity is proportional to σ_C (n_{SAM}/d_C) $\lambda_C T(E_C)$[exp ($-nd_C/\lambda_C \cos\theta$)], where n is the number of C in the SAM backbone and θ is the takeoff angle. For the inelastic mean free path of the C(1s) photoelectrons, we use λ_C = 24.5 Å.[53] Making use of these expressions, we have computed the density, n_{SAM}, for both the SAMs, and these values are also given in Table 1. Given the assumptions made here to calculate these values, we estimate that their absolute accuracy is approximately ±30%. A higher density (3.4×10^{14} vs 2.1×10^{14} molecules·cm^{-2}) is observed for the **2P** SAM. This can again be attributed to the fact that more aromatic rings lead to higher intermolecular forces which in turn account for the smaller tilt and higher packing density.[49] A density of 4.5×10^{14} molecules·cm^{-2} has been reported for a SAM of 4-[4′-(phenylethynyl)-phenylethynyl]-benzenethiol on Au,[54] which has a similar molecular structure to the **2P** SAM, but possesses a different headgroup and lacks the terminal isopropylamine group, which in our case may hinder packing of the molecules.

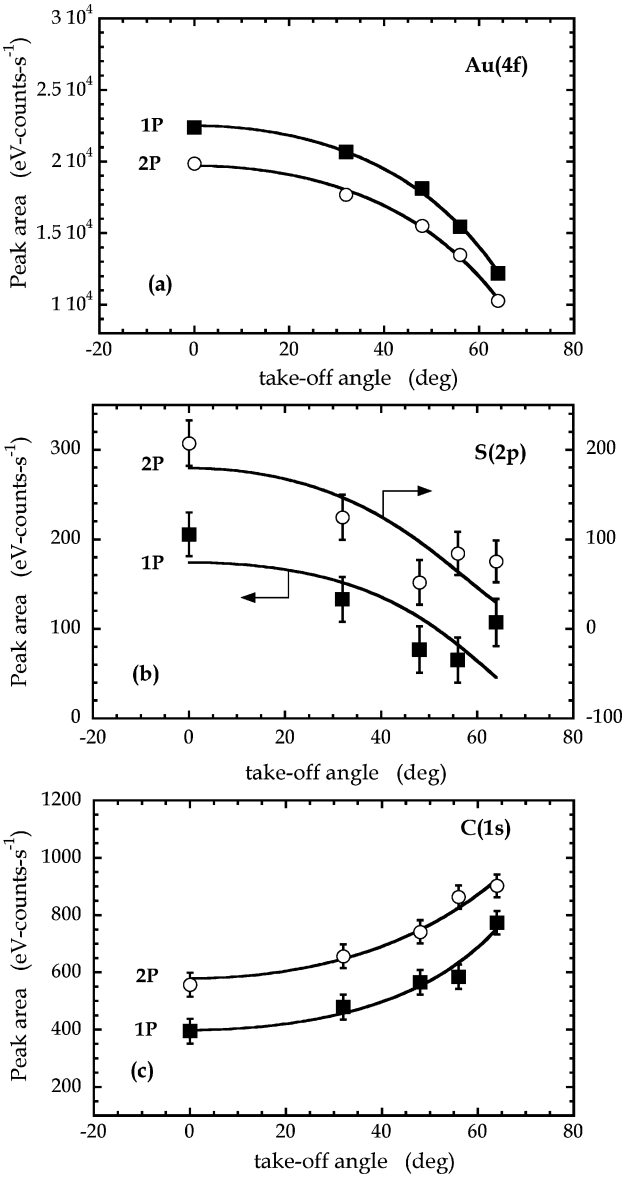

Figure 2. Integrated peak areas as a function of takeoff angle for the **1P** (filled symbols) and **2P** SAMs (open symbols) on polycrystalline Au for the (a) Au(4f), (b) S(2p), and (c) C(1s) features from XPS at T_s = 30 °C. The smooth curves represent fits of the data to models that are described in the text. The parameters found from these fits are given in the text and/or in Table S1 in the Supporting Information.

Angle-resolved XPS has been used to probe the SAMs, which is particularly valuable concerning noninvasive depth profiling of the layers. ARXPS of the Au(4f), S(2p), and C(1s) peaks have been obtained. The takeoff angle was varied from 0° to 64°. Plotted in Figure 2a are the Au(4f) integrated intensities as a function of the takeoff angle for both the SAMs we consider here. The data can be modeled as a semi-infinite (Au) substrate that is covered by a uniformly thick two-dimensional (SAM) film: $I(\theta) = I_0 \exp(-d_{SAM}/\lambda \cos\theta)$, where, I_0 is the

(49) Frey, S.; Stadler, V.; Heister, K.; Eck, W.; Zharnikov, M.; Grunze, M. *Langmuir* **2001**, *17*, 2408−2415.
(50) *Practical Surface Analysis: Volume I, Auger and X-ray Photoelectron Spectroscopy*, 2nd ed.; Seah, M. P., Briggs, D., Eds.; John Wiley and Sons: Chichester, England, 1990.
(51) Ashcroft, N. W., Mermin, N. D. *Solid State Physics*; Harcourt Brace College Publishers: Orlando, FL, 1976.
(52) Powell, C. J.; Jablonski, A. *J. Vac. Sci. Technol. A* **1999**, *17*, 1122−1126.
(53) Lamont, C. L. A.; Wilkes, J. *Langmuir* **1999**, *15*, 2037−2042.
(54) Walker, A. V.; Tighe, T. B.; Stapleton, J.; Haynie, B. C.; Upilli, S.; Allara, D. L.; Winograd, N. *Appl. Phys. Lett.* **2004**, *84*, 4008−4010.

unattenuated emission achieved at normal takeoff angle. The smaller integrated intensities for the **2P** SAM at all takeoff angles are consistent with the fact that more attenuation of the Au (4f) photoelectrons is occurring due to the presence of a thicker (and denser) overlayer. In terms of the parameters, from these data, we find $d_{SAM}/\lambda = 0.47 \pm 0.01$ and 0.49 ± 0.02 for the **1P** and **2P** SAM, respectively. These values for the parameters, as well as all values obtained in this work from ARXPS, are also given in Table S1 in the Supporting Information. In Figure 2b, we display the S(2p) integrated intensity as a function of the takeoff angle for both SAMs. In this case, it is assumed that sulfur atoms are arranged in a 2-D plane at a distance, *d*, from the SAM−vacuum interface. The expression is given by $I(\theta) = (I_0/\cos\theta)\exp(-d/\lambda\cos\theta)$, where again I_0 is the unattenuated emission achieved at normal takeoff angle A fit to the data shown in Figure 2b gives $d/\lambda = 1.69 \pm 0.57$ and 2.05 ± 0.65 for the **1P** and **2P** SAM, respectively. These values indicate that the sulfur is a significant distance beneath the surface, presumably at the SAM−Au interface. Also, the values found for d/λ increase with increasing length of the SAM. We will return to a discussion of the physical meaning of the absolute values below. Results from ARXPS of the C(1s) peak for both the SAMs are presented in Figure 2c. Here we use the following expression to model the data: $I(\theta) = I_0\,[1 - \exp(-d_{SAM}/\lambda\,\cos\theta)]$, which assumes the C is present at some constant density in a thin film at the surface and where I_0 is the C(1s) emission from a semi-infinite SAM film. Here we find that $d_{SAM}/\lambda = 0.32 \pm 0.14$ and 0.68 ± 0.12 for the **1P** and **2P** SAM, respectively. One final set of experiments was conducted to further characterize the SAMs. In these experiments, first a scan for Au(4f) was completed on a clean Au substrate, and this was followed directly by another scan on a Au substrate covered by the SAM. Again, assuming the SAM covers the surface uniformly this gives directly the quantity $I(\theta)/I_0 = \exp(-d_{SAM}/\lambda\,\cos\theta)$. We find that $d_{SAM}/\lambda = 0.21 \pm 0.01$ for the **1P** SAM and 0.29 ± 0.01 for the **2P** SAM. These values are in qualitative agreement with those found in Figure 2a, b, and c. One explanation for the disparity in d_{SAM}/λ values could be a difference in attenuation between the Au photoelectrons and those arising from C and S. For example, as C and S are both part of the SAM molecules, attenuation by the remaining portion of the molecule is assured. Such is not the case for the Au substrate, particularly for a less-than-well-packed SAM overlayer. In any event, these results are consistent with a SAM where the molecules are bound exclusively by the thiophene end of the molecule.

B. Reaction of Ti[N(CH$_3$)$_2$]$_4$ with the SAMs. The reaction of Ti[N(CH$_3$)$_2$]$_4$ with the clean Au substrate and the **1P** and **2P** SAMs has been examined using XPS. In our previous work on trichlorosilane-based SAMs,[33] the starting substrate was found to be the most reactive. In this work, the substrate was "chemical" silicon oxide, which has a high density of silanol groups at the surface. To determine if a similar phenomenon was possible in the systems examined here, we have studied the reaction of Ti[N(CH$_3$)$_2$]$_4$ with a clean Au substrate at $T_s = 30$ °C. After a 1 h exposure to Ti[N(CH$_3$)$_2$]$_4$ (dose of $\sim 1.01 \times 10^{17}$ molecules·cm^{-2}), a Ti(2p) spectra was acquired, which is displayed in Figure 3. In Figure 3, we also display the results of a 30 min exposure of the **2P** SAM to Ti[N(CH$_3$)$_2$]$_4$. It can be clearly seen that there are only trace amounts of Ti present

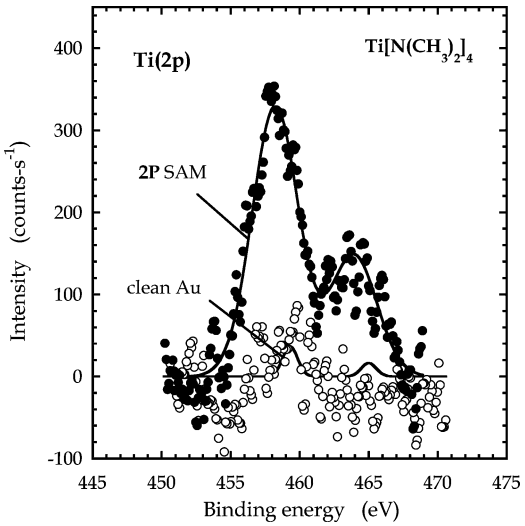

Figure 3. XP spectra of the Ti(2p) feature for clean Au and **2P** SAM surfaces, both exposed to Ti[N(CH$_3$)$_2$]$_4$ at $T_s = 30$ °C. Exposures were 1.01 and 0.50×10^{17} molecules·cm^{-2}, respectively. Spectra have been fit to two peaks using Gaussian−Lorentzian product functions.

on the clean Au substrate in comparison to the surface with the **2P** SAM. The area of the peaks can be used to estimate the surface density of Ti. First, we obtained a Ti(2p) spectrum from a reference single-crystal TiO_2 surface. The area under this peak is proportional to $\sigma_{Ti}N_{Ti}\lambda_{Ti}T(E_{Ti})$, where $\lambda_{Ti} = 20.67$ Å,[55] and $N_{Ti} = 3.2 \times 10^{22}$ atoms·cm^{-3}. The Ti atoms in the Ti[N(CH$_3$)$_2$]$_4$ adlayer are modeled as a thin film of thickness d_{Ti} and atomic density N'_{Ti}. The area under the peak from such an adlayer is proportional to $\sigma_{Ti}N'_{Ti}d_{Ti}T(E_{Ti})/\cos\theta$, assuming $d_{Ti} \ll \lambda_{Ti}$. Thus, the quantity $N'_{Ti}d_{Ti}$, which represents the Ti surface density (atoms·cm^{-2}), can be calculated directly. We find that the (temperature-averaged) saturation Ti densities on the three substrates are $0.073 \pm 0.03 \times 10^{14}$ (clean Au), $1.2 \pm 0.2 \times 10^{14}$ (**1P** SAM), and $2.1 \pm 0.2 \times 10^{14}$ atoms·cm^{-2} (**2P** SAM). A higher Ti saturation coverage for the **2P** SAM is in agreement with the results given above where a higher coverage of SAM molecules, and hence reactive endgroups, was implicated.

To examine the kinetics of adsorption, we have acquired coverage−exposure relationships for both the SAMs at two different values of T_s (30 and −50 °C). These data have been fit to first-order Langmuirian kinetics, $n_s(d\theta/dt) = S_{R,0}F(1 - \theta)$, where, n_s is the density of reactive sites (molecules·cm^{-2}), θ is the fractional surface coverage of Ti[N(CH$_3$)$_2$]$_4$, $S_{R,0}$ is the initial reaction probability, and F is the incident flux of Ti[N(CH$_3$)$_2$]$_4$ (molecules·cm^{-2}·s^{-1}). The data and the fits thereof are presented in Figure 4 for the **1P** and **2P** SAM. Using our estimates for the absolute densities of Ti and the estimated incident flux of Ti[N(CH$_3$)$_2$]$_4$, we can calculate $S_{R,0}$. At $T_s = 30$ °C, we find that $S_{R,0} = 0.024$ and 0.028 for the **1P** and **2P** SAM, respectively. At $T_s = -50$ °C, we find values of 0.010 and 0.020, respectively. Whereas the uncertainties in the absolute values are on the order of ±50%, the uncertainties in the relative values are much less, perhaps on the order of ±10%. Given these estimates, we conclude that the initial reaction probability in three of the four cases is within the experimental uncertainties. For the case that appears to deviate, the **1P** SAM at $T_s = -50$ °C ($S_{R,0} = 0.010$), we note that the fit to the model at low

(55) Seah, M. P.; Dench, W. A. *Surf. Interface Anal.* **1979**, *1*, 2−11.

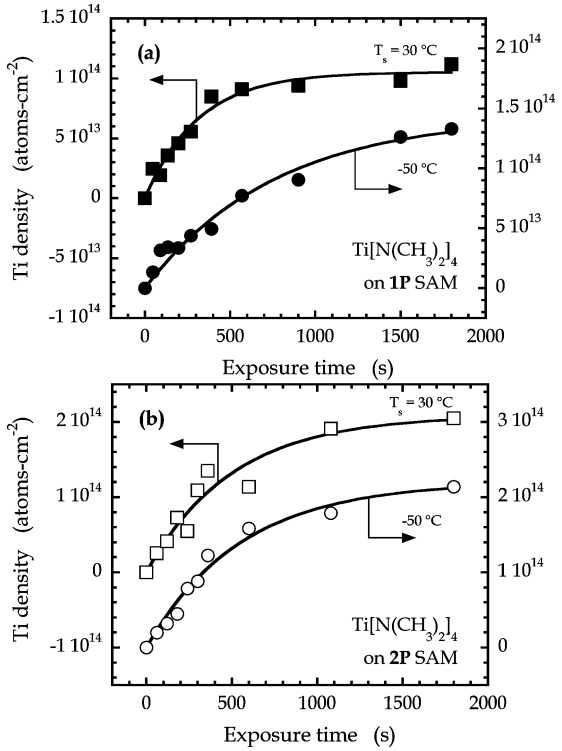

Figure 4. Coverage−exposure relationships, deduced from XPS, for the adsorption of $Ti[N(CH_3)_2]_4$ on (a) the **1P** SAM and (b) the **2P** SAM, both for $T_s = -50$ and 30 °C. The fits to the data, shown as smooth curves, are for first-order Langmuirian kinetics.

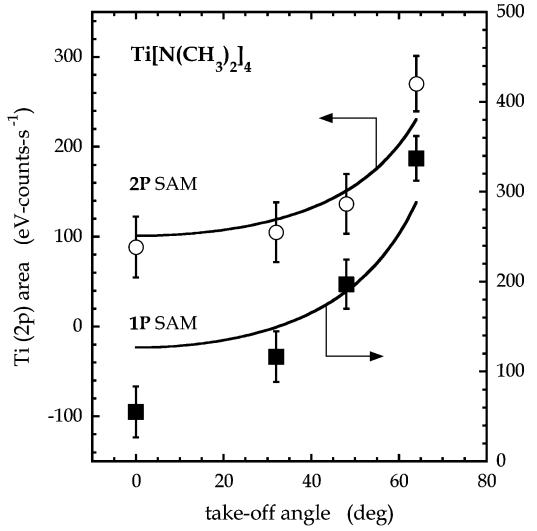

Figure 5. Integrated peak areas for the Ti(2p) region as a function of takeoff angle for a saturation exposure of the **1P** (filled symbols) and **2P** SAMs (open symbols) to $Ti[N(CH_3)_2]_4$ at $T_s = 30$ °C. The smooth curves represent fits of the data to a model that is described in the text. The parameters found from these fits are given in the text and/or in Table S1 in the Supporting Information.

coverage is not particularly good, and a simple linear fit of the first three to four data points would have revealed a larger $S_{R,0}$, closer to that implicated in the other three cases.

Angle-resolved XPS has been used to probe the spatial extent of the reaction between $Ti[N(CH_3)_2]_4$ and the SAMs, similar to what was conducted for the SAMs themselves (Figure 2). To probe for the spatial location of Ti in the adlayer, XP spectra for the Ti(2p) features have been acquired at four different takeoff angles from 0° to 64°. In Figure 5, we display the Ti-(2p) integrated intensity, plotted as a function of takeoff angle, for both SAMs and saturation exposures to $Ti[N(CH_3)_2]_4$. Clearly, for both adlayers, we see that the intensity increases as a function of takeoff angle, which points to the presence of Ti at the SAM−vacuum interface, as opposed to being buried at the SAM−Au interface. The Ti (2p) has been fit to the expression used for the S(2p) peak above (Figure 2b), namely, $I(\theta) = (I_0/\cos\theta)\exp(-d/\lambda\cos\theta)$. Here we force the quantity d/λ to be a positive definite. A fit of the data (shown by the smooth curves) gives $d/\lambda = 0.0003 \pm 0.3$ for the **1P** SAM and $d/\lambda = 0.0003 \pm 0.2$ for the **2P** SAM. From these values, we can safely conclude that all the Ti is present at the SAM−vacuum interface in both cases. Penetration, followed by reaction at the SAM−Au interface, can be ruled out on the basis of these data and is unlikely due to the negligible reactivity observed for $Ti[N(CH_3)_2]_4$ on the clean Au substrate. In summary, these results indicate that the Ti is at the SAM−vacuum interface, bound to the $-NH(i\text{-}C_3H_7)$ SAM endgroup in both cases.

Angle-resolved XP spectra of the Au(4f), S(2p), and C(1s) peaks have also been acquired from adlayers representing saturation exposures of both SAMs to $Ti[N(CH_3)_2]_4$. These experiments were conducted to determine if exposure of the SAMs to $Ti[N(CH_3)_2]_4$ resulted in significant changes in the adlayer other than reaction with the endgroup, possibly including displacement/desorption of the adsorbed molecules. These data are shown in Figure 6a, b, and c, which are identical in layout to those shown in Figure 2, and have been fit to the corresponding functional forms indicated above. A number of things are apparent upon comparison of Figures 2 and 6. First, the qualitative trends for all three peak areas for both SAMs are unchanged after exposure to $Ti[N(CH_3)_2]_4$—the Au(4f) and S(2p) peaks are attenuated, whereas the C(1s) increases in intensity at more glancing takeoff angles. These results are consistent with a situation in which significant structural rearrangement and/or ligand displacement has not occurred upon $Ti[N(CH_3)_2]_4$ chemisorption, leaving the molecules still bound to the Au surface via the thiophene linkage. Indeed, some changes in features are minimal. For example, a fit of the data for the Au-(4f) peaks shown in Figure 6a gives $d_{SAM}/\lambda = 0.46 \pm 0.01$ and 0.43 ± 0.04 for the **1P** and **2P** SAM, respectively, values essentially unchanged from those for the bare SAMs (cf. Table S1, Supporting Information).

Closer inspection of the data, however, does reveal some important differences. In particular, for the **2P** SAM, exposure to $Ti[N(CH_3)_2]_4$ resulted in a rather small increase of ~6% in the Au(4f) intensity at all takeoff angles, whereas a more substantial increase of ~21% occurred on the **1P** SAM. Although $Ti[N(CH_3)_2]_4$ chemisorption might produce SAM desorption, this seems very unlikely because the Ti species does not compete with the SAM for adsorption sites, but rather exhibits a propensity to react with the endgroup on the SAM itself. A more plausible explanation is that reaction between the Ti species and the SAM has changed the orientation of these species, making them more upright and less able to cover the underlying Au substrate. This scenario is consistent with the larger change seen for the **1P** SAM, which, from ellipsometry, consists of a monolayer that is less dense and less upright.

For the S(2p) peak, cf. Figure 6b, we find that there is a small change in the absolute intensities for the **1P** SAM upon reaction with $Ti[N(CH_3)_2]_4$, whereas there appears to be a much more

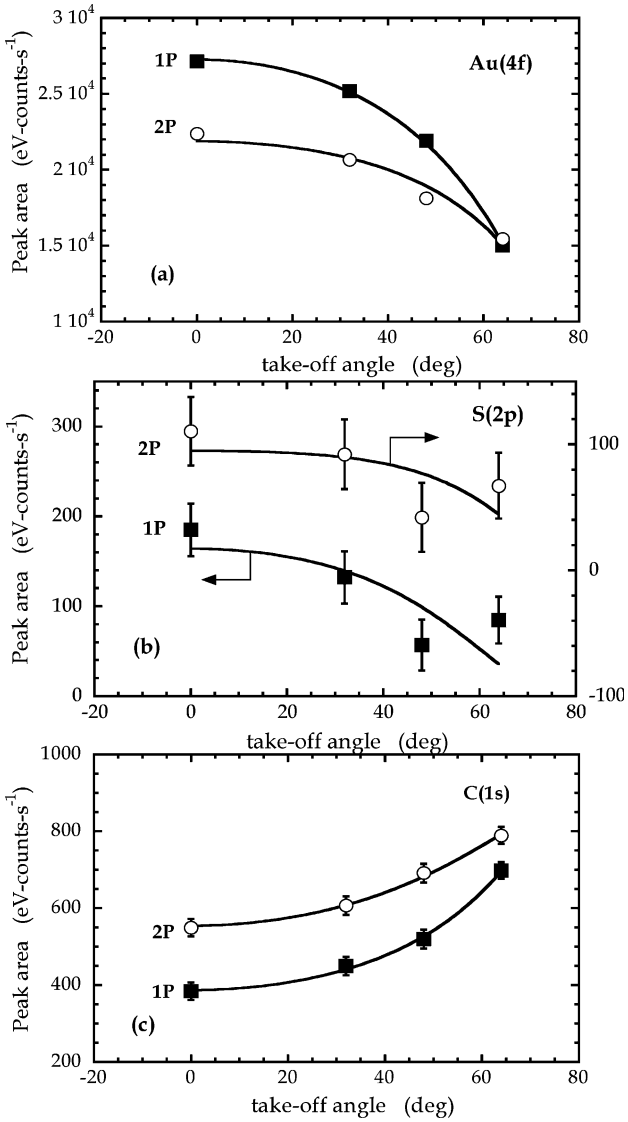

Figure 6. Integrated peak areas as a function of takeoff angle for the **1P** (filled symbols) and **2P** SAMs (open symbols) after saturation exposures to $Ti[N(CH_3)_2]_4$ at $T_s = 30$ °C for the (a) Au(4f), (b) S(2p), and (c) C(1s) features from XPS. The smooth curves represent fits of the data to models that are described in the text. The parameters found from these fits are given in the text and/or in Table S1 in the Supporting Information.

substantial (~50% at 0° takeoff angle) attenuation of this peak for the **2P** SAM. Given the results for the Au(4f) peak discussed above, differing behavior of the two layers is not unexpected. For example, restructuring of the **1P** adlayer upon reaction into a more sparse adlayer, which is also thicker, might produce minimal changes in the intensity. On the other hand, reaction and deposition leading to minimal restructuring of the **2P** SAMs could further attenuate the S(2p) signal coming from the Au−SAM interface. Finally, for the C(1s) peak, cf. Figure 6c, we find that there is minimal change in the absolute intensities (less than 5%), and fits to the data give $d_{SAM}/\lambda = 0.42 \pm 0.04$ and 0.98 ± 0.05 for the **1P** and **2P** SAM, respectively. These somewhat larger values for d_{SAM}/λ might reflect a thicker C layer due to the presence of the $N(CH_3)_2$ ligands from the $Ti[N(CH_3)_2]_4$.

To obtain more insight into the structure and composition of the adlayer formed at a saturation exposure, we further consider the results from XPS. In particular, from the C(1s) feature of

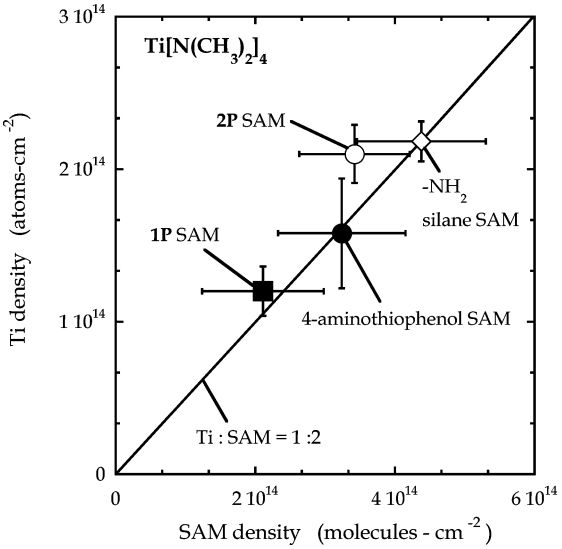

Figure 7. Relationship between the concentration of Ti in the saturated adlayers and the concentration of molecules (and functional endgroups) in the SAMs. The datum for the $-NH_2$-terminated alkylsilane is from ref 33.

the (bare) SAMs, we have been able to compute the SAM density. Likewise, following a saturation exposure to $Ti[N(CH_3)_2]_4$, we have been able to compute the density of Ti present. Combining these results allows us to calculate the Ti/SAM ratio for both SAMs. In Figure 7, we plot the Ti density vs the SAM density at saturation. Also plotted are our data for the reaction of $Ti[N(CH_3)_2]_4$ with a tricholorosilane-based alkylamine SAM on SiO_2.[33] As may be seen the ratio is ~1:2 in both cases considered here and for the alkylamine ($-NH_2$ endgroup), a result that is consistent with different scenarios. In one scenario, it can be argued that each $Ti[N(CH_3)_2]_4$ molecule is reacting with two SAMs via the $-NH(i\text{-}C_3H_7)$ group, effectively occupying all possible reactive endgroups. In another scenario, one could argue that on an average only one-half of the $-NH(i\text{-}C_3H_7)$ groups are reacting with $Ti[N(CH_3)_2]_4$. This situation is also plausible because the SAM ligands considered here are bulky and possess a relatively inflexible backbone, where steric hindrance might limit $Ti[N(CH_3)_2]_4$ to react only with every alternate reactive endgroup.

Additional insight into the stoichiometry of the adlayer can be gained by examining the N/Ti ratio. Concerning the scenarios considered above, for $Ti[N(CH_3)_2]_4$ reacting with only one-half of the SAMs present, and simple ligand exchange for chemisorption [loss of one $N(CH_3)_2$ ligand via formation of $HN(CH_3)_2$], we would expect a ratio of 5:1 in the absence of attenuation effects. Alternatively, for the case where each $Ti[N(CH_3)_2]_4$ reacts with two SAMs, again by simple ligand exchange, we would expect a ratio of 4:1. In Table 2, we give the N/Ti ratios for the saturated adlayers for both SAMs and for our previous results on the alkylamine. Also indicated in Table 2 are the substrate temperatures at which the experiments were conducted. The N/Ti ratios have been calculated after making suitable corrections for the photoelectron cross-sections. Clearly, a N/Ti ratio of approximately 3:1 is observed for both the SAMs considered here, independent of substrate temperature. At $T_s = -50$ °C, a ratio of ~4:1 is observed for the alkylamine. The ratio of 3:1 is unexpected, but nonetheless in poor agreement with the scenario where only one-half of the SAMs react with $Ti[N(CH_3)_2]_4$. Alternatively, exclusively attenuation

Table 2. Stoichiometry of the Saturated Adlayers, $Ti[N(CH_3)_2]_4$ on SAMs

substrate	SAM	substrate temperature	N/Ti
polycrystalline Au	**1P**	−50 °C	2.9 ± 0.2
	1P	30 °C	3.0 ± 0.2
	2P	−50 °C	3.3 ± 0.4
	2P	30 °C	2.9 ± 0.2
	4-aminothiophenol	30 °C	4.0 ± 0.3
SiO_2	$-NH_2$-terminated alkylsilane	−50 °C	4.0 ± 0.3
	$-NH_2$-terminated alkylsilane	30 °C	3.0 ± 0.2

effects would also seem to be insufficient to explain a reduction in the theoretical ratio of 4:1 for $Ti[N(CH_3)_2]_4$ bound to two SAMs. One remaining possibility is the additional loss of ligand via pathways that do not involve ligand exchange.

As a final point of comparison, we have examined the adsorption of 4-aminothiophenol (4-ATP) on polycrystalline Au and its reaction with $Ti[N(CH_3)_2]_4$. This molecule, which has been examined by a number of groups concerning its use as an adhesion promoter,[56−58] possesses a much simpler structure, −SH and $-NH_2$ groups separated (para) by a phenyl group. In one study,[58] from electrochemical deposition, a saturation coverage of $5.5 \pm 0.4 \times 10^{14}$ molecules·cm^{-2} was reported. As with the molecules of primary interest here (the **1P** and **2P** SAMs), we first prepared an adlayer of the SAM itself and characterized it using contact angle measurements, ellipsometry, and ARXPS. Subsequently, this layer was exposed to $Ti[N(CH_3)_2]_4$ and the layer was again characterized using ARXPS. For this adlayer, we did not attempt a characterization of the kinetics of adsorption. The results of the contact angle and ellipsometry studies are displayed in Table 1. The contact angle (sessile drop method) of 26.9 ± 3.1 is smaller than that observed for the **1P** and **2P** SAMs. The ellipsometric thickness of 10.7 ± 0.8 Å, unlike the results for the **1P** and **2P** SAMs, is larger than expected, even for a molecule bound to the surface upright (calculated length of 5.6 Å). One expects this molecule to be bound upright, and if it is bound with a higher density than the **1P** and **2P** SAMs, then it could produce a larger apparent thickness from ellipsometry due to the assumptions concerning the dielectric constant.

Concerning ARXPS of 4-aminothiophenol, the results are presented in Figure 8a, b, and c for the Au(4f), S(2p), and C(1s) peaks (pre- and postexposure) and in Figure 9 for the Ti(2p) peak (exposure was $\sim 1.01 \times 10^{17}$ molecules·cm^{-2}). As shown Figure 8, the results for ARXPS on the unreacted SAM is qualitatively similar to that observed for the **1P** and **2P** SAMs: increasing attenuation of the Au(4f) and S(2p) features with increasing takeoff angle, higher intensity for the C(1s). Again these features have been fit to the models used to fit the data in Figures 2 and 6. Shown in Figures 8 and 9 are the results for ARXPS on the SAM after reaction with $Ti[N(CH_3)_2]_4$. In Figure 9, we fit the data for the Ti(2p) peak, using the form used above in connection with Figure 5, and arrive at a value of $d/\lambda =$ 0.11 ± 0.10 for $Ti[N(CH_3)_2]_4$ on aminothiophenol, which indicates that all of the Ti is present at the SAM−vacuum interface.

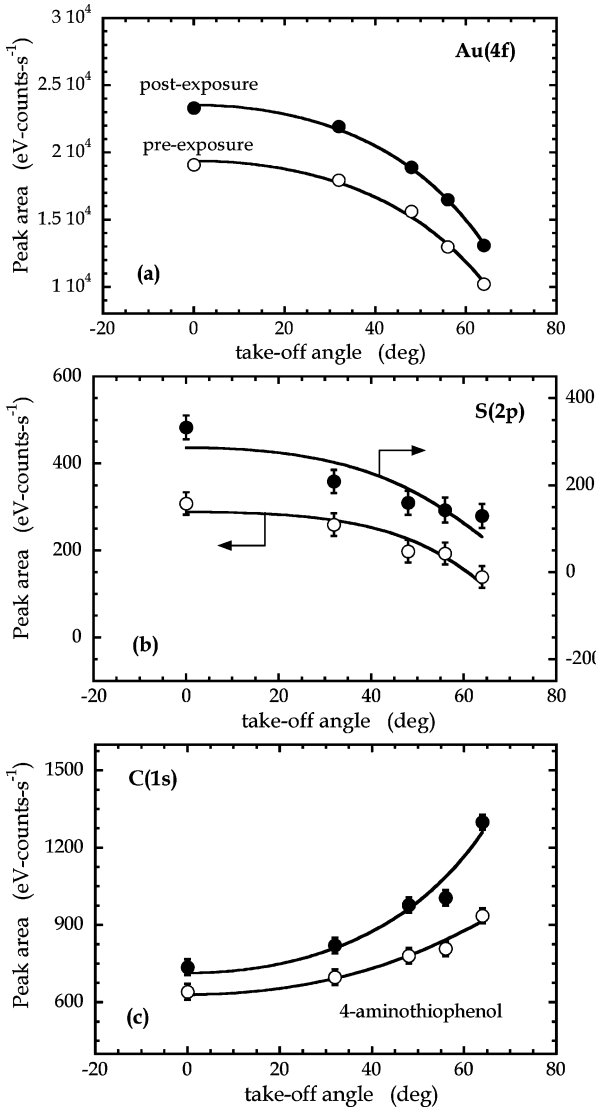

Figure 8. Integrated peak areas as a function of takeoff angle for the 4-aminothiophenol SAM on polycrystalline Au, prior (open symbols) and subsequent (closed symbols) to a saturation exposure to $Ti[N(CH_3)_2]_4$ at T_s = 30 °C for the (a) Au(4f), (b) S(2p), and (c) C(1s) features from XPS. The smooth curves represent fits of the data to models that are described in the text. The parameters found from these fits are given in the text and/or in Table S1 in the Supporting Information.

Examining the results shown in Figure 8, we observe the following: for the Au(4f) feature, a fit of the data shown in Figure 8a gives $d_{SAM}/\lambda = 0.49 \pm 0.02$ (bare SAM) and 0.45 ± 0.01 (reacted SAM), a minimal change. More interesting is the fact that we observe an increase in the Au(4f) emission at all takeoff angles after exposure to $Ti[N(CH_3)_2]_4$, where the percentage increase (21.5%) is essentially that seen for the **1P** SAM (21.2%) in the same situation. As indicated above, if chemisorption results in local densification of the adlayer about the Ti center, then this could occur in the absence of SAM desorption. For the S(2p) peak displayed in Figure 8b, we see that exposure to $Ti[N(CH_3)_2]_4$ has changed the photoemission intensity only perhaps a small amount. These results would seem to confirm that the S−Au bond is intact, even in the presence of reaction with the $-NH_2$ tailgroup. Finally, for the C(1s)

(56) Schlieben, O.; Hormes, J. *J. Synchrotron Rad.* **1999**, *6*, 793−795.
(57) Hooper, A. E.; Werho, D.; Hopson, T.; Palmer, O. *Surf. Interface Anal.* **2001**, *31*, 809−814.
(58) Batz, V.; Schneeweiss, M. A.; Kramer, D.; Hagenström, H.; Kolb, D. M.; Mandler, D. *J. Electroanal. Chem.* **2000**, *491*, 55−68.

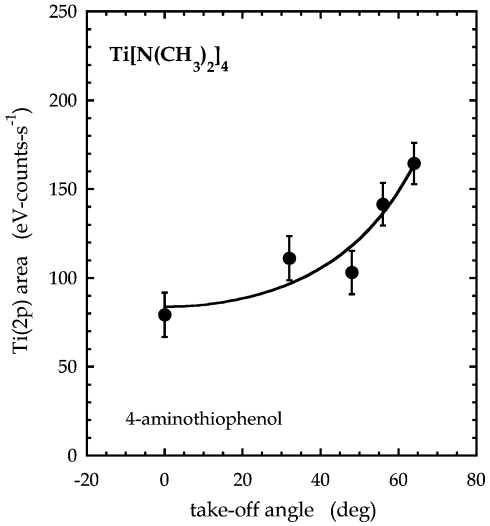

Figure 9. Integrated peak area for the Ti(2p) region as a function of takeoff angle for a saturation exposure of the 4-aminothiophenol SAM to Ti-$[N(CH_3)_2]_4$ at $T_s = 30$ °C. The smooth curves represent fits of the data to a model that is described in the text. The parameters found from these fits are given in the text and/or in Table S1 in the Supporting Information.

feature, we see from Figure 8c that the intensity increases with increasing exposure to $Ti[N(CH_3)_2]_4$. This situation is consistent with an increased amount of C in the layer due to the $N(CH_3)_2$ ligands. As discussed above in connection with Figure 6c, we found a modest (~20%) decrease in the C(1s) intensity for both the **1P** and **2P** SAMs upon exposure to $Ti[N(CH_3)_2]_4$. It is important to note that there is considerably less C in the 4-ATP (6 atoms vs 16 and 23), and a larger relative increase is expected. In terms of the parameters used to fit Figure 8c, the increase in the C fraction is about 0.88 ± 0.41 or 5.3 ± 2.5 C atoms if no SAM is lost to desorption.

As with the results for the **1P** and **2P** SAMs, XPS can also be used to quantify the stoichiometry of the adlayer: the ratios Ti/SAM and Ti/N at saturation. Following a procedure identical to that used for the **1P** and **2P** SAMs, we calculate that the absolute coverage of 4-ATP for our conditions was $3.24 \pm 0.91 \times 10^{14}$ molecules·cm^{-2}. For Ti, we estimate a saturation coverage of $1.58 \pm 0.36 \times 10^{14}$ molecules·cm^{-2}. These results are plotted in Figure 7, and we see that they are in good agreement with the other systems we have studied with $-NHR$ termination: a Ti/SAM ratio of ~1:2. For the N/Ti ratio, we find a value of $N/Ti = 4.03 \pm 0.25$ for 4-ATP and $Ti[N(CH_3)_2]_4$ adsorption at $T_s = 30$ °C. This is essentially the result we achieved with an $-NH_2$-terminated alkylsilane SAM on SiO_2 but seems to differ from the results we report here for the **1P** and **2P** SAMs and the alkylsilane at $T_s = 30$ °C, where the apparent stoichiometry was ~3:1.

Reviewing our results as a whole, we will focus on the following three important issues: (i) the kinetics of adsorption; (ii) the structure of the reacted and unreacted SAMs; and (iii) the stoichiometry of the saturated adlayer. Concerning the first of these, in previous work,[33] we examined the reactions of Ti-$[N(CH_3)_2]_4$ on alkylsilane SAMs on SiO_2. For a $-(CH_2)_{12}-NH_2$ SAM, we found initial reaction probabilities of ~0.13, 0.10, and 0.14 for $T_s = -50$, 30, and 110 °C, respectively. Focusing on the results at $T_s = 30$ °C for the **1P** and **2P** SAMs, we found values of $S_{R,0} = 0.024$ and 0.028, respectively. Although the absolute accuracy of both sets of results may be no better than ±50%, a relative comparison can be made with more confidence, as the method of calculating $S_{R,0}$ was identical in both cases. Thus, a difference in reactivity in the two cases is a factor of 3.6−4.2, with the primary alkylamine being more reactive. One expects some difference between the $-R-NH_2$ group compared to the $[-Ar-NH(i\text{-}C_3H_7)]$ group. First, the N−H bond dissociation energy of the former is expected to be higher by about 6−7 kcal·mol^{-1},[59] suggesting lower reactivity for the $-R-NH_2$ group. Additionally, a monoalkylamine species is less acidic than an *N*-alkyl aniline. Hence, if the transamination reaction were mediated by deprotonation of the incoming ligand, then the long-alkyl-chain $-R-NH_2$ species would be moderately less reactive toward substitution. On the other hand, steric effects will certainly be in play for the **1P** and **2P** SAMs (e.g., the bulkier $i\text{-}C_3H_7$ and phenyl groups), in comparison to the long-alkyl-chain $-R-NH_2$. On the basis of our results, it appears that these steric effects dominate the substitution chemistry in our system, probably influencing both the pre-exponential factor and the barrier to reaction.

Concerning the structure of the SAMs, both before and after exposure to $Ti[N(CH_3)_2]_4$, work on related systems is very limited. Most relevant are structural studies of thiophene,[46,60] and oligo(phenylene-ethynylene)[61] monolayers. STM studies[60] suggest that thiophene forms an ordered paired-row structure on Au(111), with a density of $\sim 5.2 \times 10^{14}$ molecules·cm^{-2}. However, adding methyl groups to the molecule in the case of 2,5-dimethylthiophene destroys the ability to form this ordered structure, and no ordered monolayers are observed. In the case of oligo(phenylene-ethynylene) monolayers (thiol headgroup, unfunctionalized phenyl tail group), on the basis of results from contact mode AFM,[61] a $(\sqrt{3} \times \sqrt{3})R30°$ structure was formed, which would correspond to a density of $\sim 4.6 \times 10^{14}$ molecules·cm^{-2}. Addition of a $-NO_2$ group at the central phenyl group did not seem to affect ordering of this monolayer. Finally, in this study, on the basis of results from infrared spectroscopy,[61] an average tilt angle of ~32−39° was reported.

In the work we report here, we use XPS to deduce structural properties of the monolayers. For the **2P** SAM, we estimate that the saturation density is 3.4×10^{14} molecules·cm^{-2}, which would represent a coverage of 0.245 on Au(111), consistent with a (2×2) overlayer. The ellipsometric data implies a tilt angle of $\theta = \cos^{-1}(16.6/19.6) = 32.1°$, remarkably close to that reported elsewhere for the oligo(phenylene-ethynylene). How do the results for the **1P** SAM fit into this picture? Let us assume that the **1P** SAM forms a $(2 \times m)$ overlayer, where a larger tilt angle results in $m > 2$. That is, as the tilt angle increases, the spacing between adjacent chains perpendicular to their molecular axis does not. Again making use of the ellipsometric data, a tilt angle of 58.4° is implicated for the **1P** SAM. If the spacing between the molecular axes has not changed from that for the **2P** SAM, then the increase in tilt angle would make $m \approx 2\cos(32.1°)/\cos(58.4°) = 3.23$. The density of such a layer of the **1P** SAM would be 2/3.23 that of the **2P** SAM layer, or $(2/3.23)(3.4 \times 10^{14}) = 2.1 \times 10^{14}$ molecules·cm^{-2}, exactly the result we estimate from XPS. Although this result fits perfectly into the structural model we

(59) Gomes, Jose' R. B.; Ribeiro da Silva, Maria D. M. C.; Ribeiro da Silva, Manuel A. V. *J. Phys. Chem. A* **2004**, *108*, 2119−2130.
(60) Noh, J.; Eisuke, I.; Araki, T.; Hara, M. *Surf. Sci.* **2003**, *532−535*, 1116−1120.
(61) Stapleton, J. J.; Harder, P.; Daniel, T. A.; Reinard, M. D.; Yao, Y.; Price, D. W.; Tour, J. M.; Allara, D. L. *Langmuir* **2003**, *19*, 8245−8255.

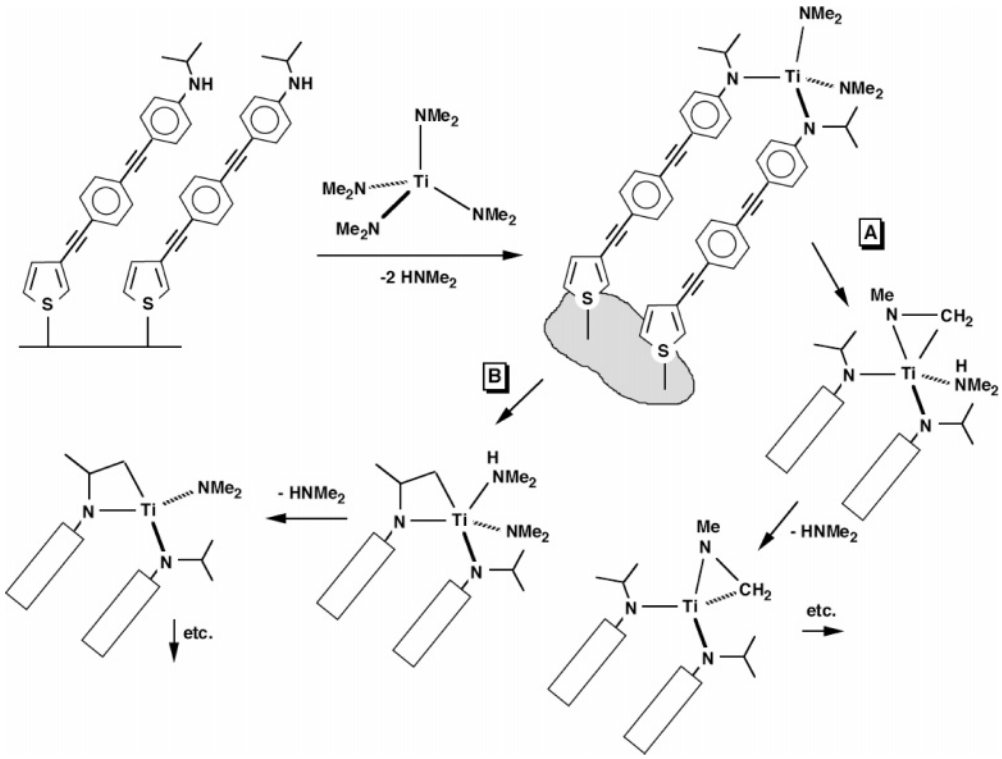

Figure 10. Possible reaction pathways for $Ti[N(CH_3)_2]_4$ reacting with the **1P** and **2P** SAMs.

have just described, we hesitate to assign too much quantitative importance to it due to the use of XPS as a quantitative measure. In a relative sense, however, XPS is quite reproducible and reliable, and these results certainly highlight the important differences in the **1P** and **2P** SAMs. In particular, the lower density and larger tilt angle implicated for the **1P** SAM, whatever the exact structure may be.

A final point of discussion concerns the stoichiometry and structure of the reacted adlayer, and we consider possible scenarios in Figure 10. Chemisorption most likely involves transamination ligand exchange reactions with the $-Ar-NH-(i\text{-}C_3H_7)$ and $-Ar-NH_2$ groups at the SAM−vacuum interface [forming $HN(CH_3)_2(g)$], and these may be facile at $T_s \leq 30$ °C. Perhaps the most striking result we have is the implied stoichiometry of the adlayer, Ti/SAM $\approx$ 1:2, for four rather different amine-terminated monolayers (cf. Figure 7). The best explanation for these results is successive ligand exchange reactions with adjacent molecules in the SAM ($-L-NHR$), forming a $(-L-NR)_2-Ti[N(CH_3)_2]_2(a)$ species. This model is a perfect fit for the results for 4-aminothiophenol and the $-NH_2$-terminated alkylsilane at $T_s = -50$ °C, based on the implicated N:Ti ratios (cf. Table 2). It is also consistent with results reported by Scott and co-workers for $Ti[N(CH_3)_2]_4$ reacting on silica surfaces,[62,63] where $(\equiv Si-O-)_2-Ti[N(CH_3)_2]_2(a)$ species were implicated. However, for both the **1P** and **2P** SAMs, and the alkylsilane at $T_s = 30$ °C, a stoichiometry of 3:1 is indicated.

A further loss of dimethylamine from $(L-N(i\text{-}C_3H_7))_2Ti[N(CH_3)_2]_2$ is a plausible way in which the predicted 4:1 ratio of N/Ti can be lowered. As discussed elsewhere,[33] if the kinetics of gas-phase unimolecular decomposition of $Ti[N(CH_3)_2]_4$ is used as a guide, then decomposition of $Ti[N(CH_3)_2]_x(a)$ species forming metallacycles and/or imines[64] is likely not kinetically feasible at $T_s \leq 30$ °C. However, for the $Ti[N(CH_3)_2]_2(a)$ fragment bound by siloxane bridges examined by Beaudoin and Scott,[63] just such a mechanism was proposed for prolonged ($\sim$10 h) "exposure" to vacuum at room temperature. Thus, including this mechanism, two pathways appear reasonable on the basis of precedent. First, a dimethylamide could abstract a hydrogen from the adjacent $Ti-N(CH_3)_2$ functionality to generate free $HN(CH_3)_2$ and an azametalacyclopropane (alternately described as a bound imine), $(L-N(i\text{-}C_3H_7))_2Ti(\eta^2\text{-}CH_2NCH_3)$ (pathway A, Figure 10). β-Abstractions from dialkylamide groups are well established in early transition metal chemistry.[63,65−70] A second possible route involves abstraction of an isopropyl group hydrogen to afford $HN(CH_3)_2$ and the azametalacyclobutane, $(L-N(i\text{-}C_3H_7))(L-\kappa^2\text{-}N,C-NCH(CH_3)CH_2)Ti(N(CH_3)_2)$ (pathway B, Figure 10). While not as common, in complexes that are sterically crowded, abstractions of peripheral hydrogens can occur concomitant with cyclometalation of the ligand.[71−73] Subsequent loss of propene from the azametalacyclobutane might occur to give $(L-N(i\text{-}C_3H_7))(L-N=)Ti(N(CH_3)_2)$, and this 3-coordinate species would be expected to add any number of CH bonds—either intra- or intermolecularly—across the imido

(62) Bouh, A. O.; Rice, G. L.; Scott, S. L. *J. Am. Chem. Soc.* **1999**, *121*, 7201−7210.
(63) Beaudoin, M.; Scott, S. L. *Organometallics* **2001**, *20*, 237−239.
(64) Dubois, L. H.; Zegarski, B. R.; Girolami, G. S. *J. Electrochem. Soc.* **1992**, *139*, 3603−3609. Driessen, J. P. A. M.; Schoonman, J.; Jensen, K. F. *J. Electrochem. Soc.* **2001**, *148*, G178−G184.
(65) Nugent, W. A.; Ovenall, D. W.; Holmes, S. J. *Organometallics* **1983**, *2*, 161−162.
(66) Mayer, J. M.; Curtis, C. J.; Bercaw, J. E. *J. Am. Chem. Soc.* **1983**, *105*, 2651−2660.
(67) Groysman, S.; Goldberg, I.; Kol, M.; Genizi, E.; Goldschmidt, Z. *Organometallics* **2004**, *23*, 1880−1890.
(68) Coles, N.; Harris, M. C. J.; Whitby, R. J.; Blagg, J. *Organometallics* **1994**, *13*, 190−199.
(69) Maury, F.; Ossola, F. *Appl. Organomet. Chem.* **1998**, *12*, 189−199.
(70) Chiu, H. T.; Huang, C. C. *Mater. Lett.* **1993**, *16*, 194−199.
(71) Simpson, S. J.; Andersen, R. A. *Inorg. Chem.* **1981**, *20*, 3627−3629.
(72) Rothwell, I. P. *Acc. Chem. Res.* **1988**, *21*, 153−159.
(73) Rothwell, I. P. *Polyhedron* **1985**, *4*, 177−200.

linkage.[74,75] In these scenarios, the ultimate N/Ti ratio would be 3:1. The feasibility of these two mechanisms is currently being investigated using quantum chemistry calculations.[76]

Independent of this proposition, however, is the unambiguous preference of $Ti[N(CH_3)_2]_4$ to react with these layers via two successive ligand-exchange reactions. As discussed above, our results for the **1P** SAM seem to indicate that the bare SAM is a low-density layer characterized by molecules closer to parallel to the surface, rather than perpendicular. Reaction with $Ti[N(CH_3)_2]_4$ would likely change that, particularly if two molecules are bound to the same Ti center. Indeed, a more upright $(-L-NR)_2-TiN(CH_3)_2$(*a*) species might be expect to occupy a smaller area of the Au surface and lead to less attenuation of the Au signal. This is, of course, exactly what we see from XPS. In contrast, the more-upright **2P** layer may lead to species covering similar amounts of the Au surface, leading to little change in attenuation of the Au signal—again, this is what is observed in XPS. More definitive conclusions concerning the structure of the reacted adlayers await direct structural studies using techniques such as STM.

IV. Conclusions

We have investigated the synthesis and characterization of conjugated thiophene SAMs with an isopropylamine endgroup, as well as their reaction with tetrakis(dimethylamido)titanium. Using contact angle measurements and ellipsometry, we have found that the shorter **1P** SAM produces an adlayer that is less dense than the longer **2P** SAM. This may be due to the nature of the intermolecular interactions in the **2P** SAM, which lead to an adlayer that involves molecules that are more upright than the **1P** SAM. These results are confirmed by results from XPS, which also indicate a higher density for the **2P** SAM. Angle-resolved XPS indicates that the molecules for both SAMs are bound to the Au surface via the thiophene headgroup, with the amine termination at the SAM−vacuum interface. Reaction of these SAMs with $Ti[N(CH_3)_2]_4$ in both cases is self-limiting, and the kinetics of adsorption are in good agreement with first-order Langmuirian kinetics. The initial probability of reaction on these SAMs is about a factor of 4 smaller than that observed on a $-NH_2$ terminated alkylsilane, which we attribute to steric effects caused by the i-C_3H_7 group on these SAMs. Angle-resolved XPS conducted after the reaction of the SAMs with $Ti[N(CH_3)_2]_4$ shows clearly that the reaction occurs cleanly with the terminal isopropylamine group, and there is no reaction at the SAM−Au interface. From XPS, we find that the stoichiometry in the saturated adlayers for both SAMs is ∼1:2 for Ti/SAM and ∼3:1 for N/Ti. These results are best explained by a model where chemisorption involves ligand-exchange reactions resulting in one $Ti[N(CH_3)_2]_x$ fragment bound to two SAMs via the isopropylamine group. Taken as a whole, these results indicate that transition metal complexes can bind very specifically and noninvasively to the endgroups on SAMs that possess a backbone that may be useful in fields such as molecular electronics.

Acknowledgment. This research was supported by the Nanoscale Interdisciplinary Research Team on Inorganic−Organic Interfaces (NSF-ECS-0210693). Additional support was provided by the Cornell Center for Materials Research (CCMR), a Materials Research Science and Engineering Center of the National Science Foundation (DMR-0079992), and the Semiconductor Research Corporation via the Center for Advanced Interconnect Science (SRC task 995.011). A.D. wishes to thank Applied Materials for a Graduate Fellowship.

Supporting Information Available: Details of the experimental procedures including materials used, synthesis, as well as all assignments of the chemical shifts from NMR for the thiophene ligands, substrate preparation, characterization of SAMs, and the adsorption kinetics experiments; and values for all the parameters obtained from ARXPS curve fits both before and after exposure to $TiN[(CH_3)_2]_4$. This material is available free of charge via the Internet at http://pubs.acs.org.

JA054378E

(74) Bennett, J. L.; Wolczanski, P. T. *J. Am. Chem. Soc.* **1997**, *119*, 10696−10719.
(75) Slaughter, L. M.; Wolczanski, P. T.; Klinckman, T. R.; Cundari, T. R. *J. Am. Chem. Soc.* **2000**, *122*, 7953−7975.
(76) Haran, M. K.; Clancy, P. Personal communication.